NASA TECHNICAL MEMORANDUM

NASA TM X-71465

NASA TM X-71465

PLUME MASS FLOW AND OPTICAL DAMAGE DISTRIBUTIONS FOR AN MMH/N_2O_4 RCS THRUSTER

by Ernie W. Spisz, Robert L. Bowman and John R. Jack
Lewis Research Center
Cleveland, Ohio 44135

TECHNICAL PAPER proposed for presentation at Seventh Space Simulation Conference cosponsored by the American Institue of Aeronautics and Astronautics, American Society for Testing and Materials, and the Institute of Environmental Sciences
Los Angeles, California, November 12-14, 1973

PLUME MASS FLOW AND OPTICAL DAMAGE DISTRIBUTIONS FOR AN MMH/N_2O_4 RCS THRUSTER

by Ernie W. Spisz, Robert L. Bowman, and John R. Jack

National Aeronautics and Space Administration
Lewis Research Center
Cleveland, Ohio

ABSTRACT

The data obtained from two recent experiments conducted in a continuing series of experiments at the Lewis Research Center into the contamination characteristics of a 5-pound thrust MMH/N_2O_4 engine are presented. The primary objectives of these experiments were to establish the angular distribution of condensible exhaust products within the plume and the corresponding optical damage angular distribution of transmitting optical elements attributable to this contaminant. The plume mass flow distribution was measured by five quartz crystal microbalances (QCM's) located at the engine axis evaluation, on a circle with a radius of 35 cm from the nozzle exit plane, and at angles of 0, 30, 45, and 90 degrees. The fifth QCM was located above the engine and 15° behind the nozzle exit plane. The optical damage was determined by ex-situ transmittance measurements for the wavelength range from 0.2 to 0.6 μm on 2.54 cm diameter fused silica discs also located at engine centerline elevation and at angles of 5, 12, 20, 30, 38, 58, and 85 degrees. Both the mass deposition and optical damage angular distributions followed the expected trend of decreasing deposition and damage as the angle between sensor or sample and the nozzle axis increased. A simple plume gas flow equation predicted the deposition distribution reasonably well for angles of up to 55 degrees. For angles greater than 55 degrees, the measured deposition distribution indicated greater gas flow than that predicted theoretically. The optical damage measurements also indicated significant effects at large angles.

INTRODUCTION

Of the many possible sources of contamination that can occur to surfaces and components on spacecraft, the exhaust plumes from reaction control system (RCS) thrusters presents one of the more serious threats. Yet only very limited quantitative data are available on contamination effects from these thrusters. The lack of data is due to the experimental difficulties encountered in simulating the proper space environment, and the inherent problems associated with the sophisticated measurements and control systems required to obtain data. For example, in order to eliminate the interaction between the environmental facility and the thruster plume, it is necessary to resort to large, clean vacuum facilities having large pumping speeds for all gases including hydrogen. This invariably requires large liquid helium cryopumped systems and large distances between the experiment and the measuring instrumentation with the attendant instrumentation wiring and signal conditioning problems. In addition, compromises must frequently be made in the experimental procedure due to facility characteristics

and the logistics and economics of the cryogenic fluids required for operating such facilities.

During the past several years the NASA Lewis Research Center has been conducting general studies on contamination effects due to small, control system thrusters. A detailed description of the facility, thruster and the results from previous tests have been presented in references 1 through 6. Basically these studies have utilized a 5-pound thrust, MMH/N_2O_4 engine that is fired in a 2 x 4 meter liquid helium cryopumped space simulation facility. The thruster is fired in a pulse-mode duty cycle that is not only typical of control system thrusters but is also compatible with the pumping capabilities of the LHe cooled space simulation chamber to maintain a suitable environment.

The purpose of this paper is to report data which have been obtained from two recent tests in this study. These two tests, though similar in concept, were very different in terms of objective, thruster firing mode and instrumentation. The primary objective of the first test was to establish the angular distribution of contamination effects (optical damage) due to nozzle exhaust products as measured by transmittance changes on a series of fused silica discs located around the engine. The primary objective of the second experiment was two-fold: (1) to measure contamination effects on solar cells and various other spacecraft materials and surface coatings, and (2) to determine the angular distribution of condensible products within the exhaust plume as measured by water-cooled quartz crystal microbances (QCM's). Only the angular distribution of the optical damage from experiment 1 and the angular distribution of the condensible deposits from experiment 2 will be presented. The contamination effects on solar cells and various materials from experiment 2 are presented in reference 7.

FACILITY AND EXPERIMENTS

Facility: The experiments were carried out in the 2 x 4 meter liquid-helium-cooled space simulation chamber described in reference 6. The engine and the experiment package are located within the space simulator as shown in figure 1. The engine is a pressure-fed, bipropellant, single/doublet unit with a stainless steel, radiation-cooled nozzle. The fuel is MMH and the oxidizer is N_2O_4. The thruster is fired in a horizontal direction toward the liquid helium-cooled wall. A gaseous argon leak is introduced into the simulator at the thruster location to cryotrap the hydrogen released during thruster firing (see ref. 6 for a discussion of this effect). The 5-pound thrust engine is generally fired in a pulse-mode with an ON-time of less than 200 msec, and OFF-time greater than 100 msec, and in a train of pulses limited to a total ON-time of less than 500 msec. This ON-time limit insures that proper space simulation is maintained at all times.

Included within the facility at various locations are fast response vacuum gauges to monitor the response and pumping characteristics of the facility. With liquid helium-cooled walls, the facility pressure is less than 1×10^{-9} torr during nonfiring periods. Prior to thruster firing, the gaseous argon leak is introduced and the tank pressure rises to an equilibrium value of 6×10^{-7} torr. When the thruster is fired, the tank pressure increases momentarily to 5×10^{-5} torr.

but within 3 minutes recovers and returns to the steady value of 6×10^{-7} torr.

Experiment 1: A schematic drawing of the test plane showing the pertinent details for experiment 1 is shown in Figure 2a. There are ten, 2.54 cm diameter, fused silica samples mounted around the thruster at the engine centerline level. The primary objective of this test was to establish the angular distribution of the effect of the plume contamination as measured by changes in the transmittance of the fused silica samples. The transmittance measurements are made ex-situ after the completion of the experiment.

The testing program for experiment 1 consisted of firing the 5-pound thrust engine on four days during which 1241 pulses of 50 msec duration were accumulated for a total exposure time of 62 seconds. The specific firing mode that was used during this test consisted of a train of 8 consecutive 50 ms pulses with 100 msec between pulses; a train was repeated every 7 minutes and approximately 40 trains were fired during 6 hour period, on each of the four firing days.

Experiment 2. A schematic drawing of the test plane showing the pertinent details for experiment 2 is shown in figure 2b. There are five, 2.54 cm diameter fused silica samples, and four QCM's mounted around the thruster at engine center line level. There is also one QCM mounted above the engine and 15° behind the nozzle exit plane. The primary objectives of this test were: (1) to establish the contamination effect to solar cells and various spacecraft materials and coatings mounted on a horizontal pallet which is located 10 cm off the engine centerline to simulate a spacecraft surface, and (2) to establish the plume deposition distribution as measured by the five QCM's. In addition, the five fused silica samples were used to obtain optical damage data to supplement Experiment 1 data.

The test program for experiment 2 consisted of firing the engine on 6 days during which 5375 pulses of 14 msec duration were accumulated for a total exposure time of 73 5 seconds The engine firing mode consisted of a train of 25 consecutive 14 msec pulses with 100 msec between pulses; a firing train was repeated every 7 minutes and approximately 36 trains were fired each day during a 6 hour period. This particular pulse firing mode was suggested by the NASA-MSFC Skylab Project office as being typical of a Skylab duty cycle.

INSTRUMENTATION

QCM Measurements: QCM's are being used extensively for flight and ground test contamination experiments (refs. 8, 9, and 10). These devices are capable of sensitive, real-time measurements of the mass depositing or leaving the surface of the sensing crystal. The crystals of the QCM's used herein (shown in figure 3) have a diameter of 1.27cm, a thickness of 0.25 mm, and an exposed surface area of approximately 0.45 cm^2. The crystals are cut on the AT-plane, are silver coated and have a natural resonant frequency of 5 MHz. The measured output of the QCM is a "beat frequency" which is composed of the 5 MHz sensing crystal frequency mixed with a reference oscillator frequency which is slightly greater than the crystal frequency. Mass addition to the crystal

causes a decrease in the crystal frequency and a corresponding increase in the beat frequency. The sensitivity of the measuring system is ≈1 Hz which corresponds to a mass addition on the crystal of .018 $\mu gm/cm^2$. Temperature control is provided for the crystal holder by a recirculating water supply to minimize temperature effects on crystal frequency. References 10 and 11 present further detail on QCM characteristics and their application for contamination monitoring.

Optical Damage Measurements: Transmittance measurements on the fused silica samples were made ex-situ, after the completion of the experiment by two independent spectrometer systems. The two systems are: (1) a MgO coated integrating sphere with a lithium-fluoride prism monochromator and (2) a 1 meter, 15^0 Robin mount ultraviolet (uv) scanning spectrometer with a 590 groove per millimeter grating.

The integrating sphere system utilized the sample-in/sample-out technique with the sample located at the inlet port of the sphere. The transmittance measurements made with this system are hemispherical transmittance in that all of the radiation transmitted through the sample is collected and measured. The transmittance measurements were made over the wavelength range from 0.34μm to 2.5μm.

The UV spectrometer measurements also utilized the sample-in/sample-out technique with the sample located at either the inlet or exit port of the instrument. The transmittance measurements (Experiment 2 only) made with the sample located at the exit port are hemispherical transmittance similar to the integrating sphere measurements. With the sample located at the inlet port, the measurements are directional transmittance in that only the radiation transmitted along the optical axis of the 1 meter spectrometer is measured. These transmittance measurements were made over the wavelength range from 0.20μm to 0.6μm.

RESULTS AND DISCUSSION

Mass Deposition Measurements: In general, the mass deposition process as indicated by the QCM measurements appeared to be erratic. Many unexplainable events were recorded during the experiment and the QCM response to each engine firing was not consistently reproduceable. This general comment is not intended to reflect unfavorably on the quality or usefulness of the recorded data, but to indicate that some difficulty was encountered in the analysis of the data to obtain useful information.

The primary difficulty encountered in analyzing the QCM data was the non-repeatability of the initial and net deposition rates which occurred with each engine firing so that representative rates could be confidently determined for each QCM in order to establish an angular deposition distribution. The poor repeatability is attributed primarily to the vertical orientation of the crystal surface and the high crystal temperature (≈15^0C). At these temperatures the deposits which collected on the crystal were undoubtly liquid; and long time accumulation would cause large droplets to form. These droplets could either flow off the crystal surface or result in non-uniform deposits on the crystal surface and cause discontinuous events to be indicated by the sensor. Further-

more, bombardment of the vertical crystal surface by the frozen or liquid exhaust particles could dislodge the residual mass on the crystal surface and result in a net decrease in the sensor output during a thruster firing period. Such events did occur frequently for QCM's which were located in the regions of high gas flow. As a result of the uncertainty of events and our lack of understanding of the real phenomena which occurred, it was necessary and useful to consider the analysis of the data in terms of an ideal QCM response.

Figure 4 presents a select set of actual experimental data illustrating, for one location, the ideal QCM response to the pulse-mode engine firing. Figure 4 is a continuous time record of the 45 degree QCM for six consecutive engine firings which occurred over a period of approximately forty-five minutes. The measured output (or response) of the QCM is the beat frequency in Hz. As material is deposited or added to the crystal surface, the beat frequency increases. The step-wise character of the recorded trace indicates an initial addition of material to the crystal surface at the instant the engine is fired in a train of twenty-five, 14 msec pulses. The step increase is the total accumulated deposits for the total train of 25 pulses which occurs over a period of 2.75 seconds (twenty-five, 14 msec firing pulses with 100 msec between pulses). The first step increase shows an initial deposit corresponding to a beat frequency change of ≈100 Hz. The 100 Hz beat frequency is a mass change of $1.80 \mu gm/cm^2$. After the initial step change, there is a gradual decrease in beat frequency over the subsequent seven minute, non-firing recovery period due to evaporation or sublimation of the deposited material. After seven minutes, the engine is again fired in a similar train of twenty-five, 14 msec pulses with a corresponding initial step increase in beat frequency of ≈100 Hz again and the subsequent slow evaporation or sublimation during the seven minute non-firing recovery period. This stepwise change is repeated every seven minutes for the six firing cycles. For the six trains, the initial beat frequency change ranged from 90 to 120 Hz (1.62 to $2.16 \mu gm/cm^2$).

The data of interest in figure 4 are the initial step change in the best frequency for each firing train, and the net or long term accumulation of deposits on the crystal surface that eventually could degrade the optical characteristics of nearby surface components. The net deposition or accumulation of mass on the sensor is indicated by the dotted line in figure 4. For the six engine firings, a net change of 60 Hz was measured corresponding to an average change of 10Hz per firing.

During each firing train, the sensor is exposed to the engine plume products for a total of 0.35 seconds (ON-time). Therefore, the rate of change in the initial beat frequency based on a per second of plume exposure time ranged from 257 to 343 Hz/sec of exposure. (The corresponding mass deposition rates are 4.63 to 6.17 $\mu gm/cm^2/sec$) These measured initial deposition rates may be lower than actually occurs because the data-taking process was unable to measure the peak frequency change, and measured a somewhat lower value after the evaporation process had started.

The net deposition change of 10 Hz for a train fired every 7 minutes results

in a net deposition rate of 0.0238 Hz/sec or 10 Hz/train. The corresponding mass rates are 0.00043μgm/cm^2/sec and 0.180μgm/cm^2/train. As can be noted in Figure 4, the OFF-period of 7 minutes is not sufficient for the total deposited mass to evaporate or sublimate and reach an equilibrium value. A longer period between firings would have permitted more deposited material to leave the crystal surface and resulted in a significantly smaller net deposition rate. Conversely, a shorter time between firings would have resulted in a much larger rate.

The precedeing discussion of the QCM response describes the material deposition phenomena on the QCM's for pulse-mode firing under the least complicated conditions. i.e. effects such as impact, mass build-up, and coalescing of contaminant droplets do not affect the deposition/evaporation process which is considered to occur. QCM response characteristics similar to that shown in Figure 4 have been measured repeatedly in previous experiment for many consecutive firing trains and for different pulse-mode duty cycles. However, it should be emphasized that such responses did not occur for all firing trains nor did it occur for all QCM's during this experiment.

To illustrate the variation in initial deposition rates that were measured throughout the test, Figure 5 shows the initial change in the beat frequency for the five QCM's. During the course of experiment 2, the thruster was fired for 225 firing trains which consisted mainly of twenty-five, 14 msec ON/100 msec OFF pulses. Data are not shown for every pulse train for two reasons: (1) data were not taken for every firing train, and/or (2) the beat frequency showed either no change or a decrease during the firing period. Only that data which showed a net positive step increase of 1Hz or greater in beat frequency is included in Figure 5. As can be noted, the range of the beat frequency change is considerable for each of the QCM's.

The data for the 0^o QCM, which is located directly on the nozzle axis, were the most difficult to interpret. After the fifth firing train on the first firing day, this QCM accumulated a mass deposit corresponding to a beat frequency change greater than 100 KHz. (This is the maximum change recommended by the sensor manufacturer, ref. 11). During the subsequent days of the experiment, the deposited material either evaporated, sublimated, dripped or was knocked from the crystal surface and consistent measurements were obtained intermittently. The initial beat frequency changes as shown in Figure 5 ranged from 110 to 9800 Hz. The average of all the measured values was 2544 Hz (46μgm/cm^2/per firing train). A value of 2156 Hz was obtained for exposure of the uncontaminated crystal to the first firing train. The first train, which was used to establish the engine combustion parameters, consisted of four, 50 msec pulses for a total exposure time of 200 msec as compared to the 350 msec exposure time obtained for the twenty-five, 14 msec pulses. Extrapolating the deposition change for the four, 50 msec pulse train to the twenty-five, 14 msec pulse train by the ratio of ON-time; the corresponding beat frequency change for the first train would have been 3773 Hz. The comparison of this value with the average change of 2544 Hz for all the measured trains gives confidence to the average value and indicated that useful data could be obtained even though the crystal had exceeded its maximum mass build-up early in the test.

Reference 12 predicts that large amounts of incomplete combustion products will occur on the nozzle axis which could explain the extreme events which were measured by the 0^{o} QCM. (A practical recommendation obtained from this data is to eliminate the 0^{o} QCM in future experiments.)

The 30^{o} QCM data were considerably more consistent than the 0^{o} QCM data. The initial change in beat frequency ranged from 43 to 1700 Hz. The average value for all the measure data points was 390 Hz. The events recorded by this QCM tended to become more erratic as the experiment progressed and the total exposure time and accumulated deposits on the crystal increased. The deteriorating response of the QCM with exposure time was attributed to the significant accumulation of mass on the sensor surface. By the 175th firing train, the QCM indicated a total mass accumulation corresponding to a beat requency change greater than 100 KHz No further data were obtained with the QCM after the 100 KHz level had been reached.

The 45^{o} QCM data were by far the most consistent and reproducible of the QCM's The initial change in beat frequency ranged from 17 to 120 Hz with most of the data occurring in the 40 to 60 Hz band. The average value of all the data points is 49 Hz

The 90^{o} QCM also operated consistently throughout the complete experiment. At this location the initial change in beat frequency ranged from 1 to 21 Hz with an average value of 3 Hz. Data are shown in Figure 5 for only a frequency change greater than 1 Hz which is considered to be the maximum resolution of the sensor system. Many engine firings resulted in no change or a negative change in heat frequency during the firing period. These changes are not shown and were not considered in determining the average value of the initial beat frequency change.

The 105^{o}QCM located above and behind the engine axis also provided consistent data throughout the experiment. The initial beat frequency change ranged from 1 to 9 Hz with an average value of 2 Hz. Again only frequency changes greater than 1 Hz are shown and many firings resulted in no increase or a decrease in the beat frequency.

In order to establish the angular distribution of the condensible products within the exhaust plume the average values of the initial change in beat frequency shown in Figure 5 are plotted in Figure 6. The data points are divided by the 0^{o} QCM value to obtain a normalized distribution for comparison with a theoretical plume gas flow calculated for an exhaust gas with a specific heat ratio of 1.28 and a nozzle area ratio of 40 which corresponds to the values for the experimental engine. The comparison between the data and the calculated distributions is reasonable for off-axis angles up to 55 degrees. However, for angles greater than 55 degrees the trend in the measured data indicates considerably higher deposition than that predicted by the gas flow from reference 13. This result is consistent with the experimental data of reference 14 which also showed significant back-flow for an expanding plume of unreacting N_2 and CO_2

gases. The faired curves selected from reference 14 are for a 15 degree nozzle with an area ratio of 60 and a plenum pressure of 3.2 psia. The trend indicated by the data, herein, and the data of reference 14 are similar and both show that significant back-flow can occur.

From a contamination viewpoint, however, it is not necessarily the total plume gas flow or the initial deposition rate which is of importance, but rather the deposits which "stick" or remain on a surface for long time periods. Such deposits can subsequently result in optical degradation and alter the operational characteristics of spacecraft surfaces and components. Referring to Figure 4 it is the net deposition rate of 10 Hz per firing train that can result in long term contamination effects. The measurement of the net deposition rate, however, was even more difficult and the interpretation of the data more qualitative than that encountered in the initial mass deposition data. Only very limited residual net deposition data were obtained. The limited data that were selected as suitable for determining net deposition rates are shown in Figures 7a, 7b, and 7c, for the 30^{o}, 45^{o} and 90^{o} QCM's. The data points that are shown are the QCM frequency just prior to each engine firing. These data were selected because of the consistent increasing trend shown by the data over a time period of one hour (or approximately 8 consecutive trains). The net deposition rate is determined by the rate of increase of this set of data and (for purposes here) is approximated by a linear fit of the data points. The primary difficulty encountered in obtaining net deposition rates was the temporal instability of QCM sensors of 100 Hz/Hr. (ref. 11), the small net deposition which occurred for the firing mode being studied, and the limited resolution ($\approx$1 Hz) of the measuring system.

For the 30^{o} QCM, three net deposition rates of 11, 20, and 89 Hz/firing train were obtained. For the 45^{o}QCM, five net rates of 9, 16, 20, 22 and 25 Hz/firing train were obtained. While for the 90^{o}QCM no rates were obtained and only a very slowly varying frequency change occurred which could not be distinguished from the expected drift of the sensor system. Similarly no data could be obtained for the 105 degree QCM. The primary conclusion which can be drawn from these data is the comparison of the average measured net deposition rates of 40 and 18 Hz/firing train between the 30^{o} and 45^{o}QCM. The change from 40 to 18 Hz/firing train (or a factor of 2) between the two locations is significantly less than the ratio of the average values for the initial deposition rates from Figure 4 of 390 to 49 Hz/firing pulse (or factor of 8). If this trend of a smaller difference between the 30^{o} and 45^{o}QCM is real, the net deposition distribution would be considerably flatter than the initial deposition curve in Figure 6.

At this point in our study, however, it must be concluded that the net deposition rate data are only qualitatively useful because of many uncontrolled effects such as crystal surface temperature, simulator environment pressure (vacuum), crystal surface history, existing residual deposits, and time between firing pulses all of which can significantly affect the mass which will remain on the crystal for long periods of time. In addition, significant differences will occur during the zero-gravity conditions of real space flight. These results,

however, are useful for providing insight into the trends which may occur for long term contaminating effects on samples.

Optical Damage Measurements· Figure 8 shows ex-situ 40x photomicrographs of four of the contaminated fused silica samples after the completion of Experiment 1. The appearance of the contaminant is a qualitative indication of the contamination effect as it is influenced by sample location. At the 5 degree angular location (sample not shown) the contaminant occurs as large, irregular shaped puddles with the major dimension greater than 500 μm. The residue exists as a clear, viscous liquid. At the 20° position, the large irregular shaped puddles do not exist but rather smaller, more circular droplets primarily in the 50 to 500 μm diameter range occur. At 38 degrees, the droplets are smaller (20 to 200 μm) and widely spaced over the sample surface. At 56 degrees the droplet size has diminished to the 10 to 50 μm range and the contaminant is becoming more evenly distributed over the sample surface. At the 85 degree location, the sample surface is almost uniformly covered by very small, tightly packed droplets in the 2-10 μm range. The contaminant creates a dry, fog-like appearance on the sample. Ex-situ transmittance measurements were made on the fused silica samples shown in Figure 2a and 2b after the completion of each experiment to establish the optical damage (or change) which occurred, and to establish the angular distribution of these changes around the engine.

Figures 9 and 10 show the measured changes in directional and hemispherical transmittance of the samples as a function of wavelength and sample location. Experiment 1 contains a more complete series of samples than does Experiment 2, other requirements in Experiment 2 limited the number of samples that could be installed. Experiment 2 data is intended mainly to supplement the Experiment 1 data in that they include hemispherical transmittance measurements below 0.34 μm which were not obtained in Experiment 1 or in previous data (reference 3 and 4).

The transmittance data are presented in terms of a normalized transmittance ratio which is defined as

$$\left(\tau_c/\tau_a\right)_{NORM} = \left| e^{(r/r_c)^2 \ln\left(\tau_c/\tau_a\right)_{MEAS.}} \right|$$

where τ_c and τ_a are the transmittance of the contaminated and clean sample; r is the distances between a sample and the nozzle exit center, and r_c is the distance between a reference sample and the nozzle exit center. The reference sample has been selected as the sample nearest the nozzle axis. (A qualitative justification for the applicability of this normalization parameter is given in reference 3. It is based upon the Lambert-Bouger Law of absorption and a simple source flow distribution for the nozzle.) The normalization parameter $(\tau_c/\tau_a)_{NORM}$ is used because of the different sample distances and the more general angular distribution that can be achieved by normalizing the data to a common distance.

The data shown in Figure 9 and 10 show a consistent trend of increasing contamination effect with decreasing wavelength for both directional and hemispherical transmittance and the expected decreasing effect as the angle between sample location and nozzle axis increases. For wavelengths greater than 0.3μm, the hemispherical transmittance data (which include only absorption losses) showed, in general, a lesser change than do the directional transmittance data which include both absorption and scattering losses.

In addition to these general trends, the following qualitative conclusions can be made from the data obtained for both experiments:

1. The magnitude of the changes is greater for the experiment 2 (14 msec pulse) data than for the experiment 1 (50 msec pulse) data indicating the possibility of greater contaminating effects with the shorter ON-time (14 msec) pulses.

2. The change in hemispherical transmittance for wavelengths longer than 0.5μm is negligible in both sets of data indicating only minor absorption effects by the contaminant in the longer visible wavelength region.

3. The large changes in hemispherical transmittance at wavelengths shorter than 0.4μm obtained in Experiment 2 indicate primarily strong absorption effects by the contaminant. The similarity between the hemispherical and directional changes indicate that only minor scattering effects occur at the short wavelengths.

Figures 11 and 12 show the data from Figures 9 and 10 as a function of angular location to illustrate the angular distribution of the transmittance changes for wavelengths of 0.20, 0.26, 0.34 and 0.48μm. The curves show the general trend of increasing effect with decreasing angle and shorter wavelength.

For Experiment 1, the angular distribution for only directional transmittance is shown. The similarity of the data for the samples to the right and left of the nozzle axis indicates a fairly uniform distribution of the exhaust products. For wavelengths shorter than 0.30μm both sets of data show that the changes at large angles are quite noticeable and are greater than 10 per cent at angles of 85 degrees. However, for wavelengths greater than 0.48μm, the effects are negligible except for samples which are within an 18 degree cone (which contains the bulk of the nozzle exhaust products).

For Experiment 2 both directional and hemispherical transmittance distributions are shown for the samples on the left side of the nozzle axis. The trends and levels are similar for both sets of data. Changes greater than 30 percent are measured at wavelengths of 0.20μm for samples located as much as 85 degrees off the nozzle axis. The damage noted in the Experiment 2 data is greater than that for the Experiment 1 and is probably attributable to the shorter firing pulse.

CONCLUSIONS

Data from two recent experiments were presented to establish the angular distribution of the plume mass deposition and the resulting optical damage (transmittance change) on fused silica samples for pulse-mode firing of a 5-pound thrust, MMH/N_2O_4 RCS thruster. The mass deposition measurements were obtained by quartz crystal microbalances located at 0, 30, 45, 90, and 105 degrees off the nozzle axis. The optical damage data were determined by ex-situ transmittance measurements on 2.54 cm diameter fused silica discs located at 5, 12, 20, 30, 38, 56 and 85 degrees. The data, though somewhat qualitative indicated the following results:

Mass Deposition Distribution. The mass deposition measured by the QCM's indicated the expected distribution of decreasing deposition rates as the angle between sample and nozzle axis increased. A comparison of the initial deposition data with a simple plume gas flow equation indicated that reasonable relative correlation was obtained for angles up to fifty-five degrees. For angles greater than fifty-five degrees, the angular distribution of the QCM measurements indicated considerably greater deposition rates than the gas flow predicted by theory. Mass deposition values as large as 10^{-3} of the nozzle centerline value were measured at angles greater than 90° indicating that plume back-flow sufficient to cause significant optical damage to surfaces or components generally considered not within the plume boundaries may occur.

Some limited net deposition data were obtained and indicated that the material which did not evaporate or sublimate from the QCM crystal surface seven minutes after exposure to the thruster firing was considerably less than the material initially condensed on the crystal surface. An angular distribution of the net deposition data, which are directly related to contamination effects, could not be obtained because of limitations in the experiment, sensors, and data gathering systems.

Significant and unpredictable events were noted by the QCM measurements for what was considered to be a stable and repetitive pulse-firing mode. These variable events were attributed to the vertical placement of the QCM crystal surface in this experiment and the random impact effects which can occur when the crystal surface in this position is bombarded by the exhaust products from the thruster. The combustion process during the 14 msec ON-time pulse was undoubtedly incomplete and resulted in large amount of unreacted exhaust products.

Optical Damage Distribution. The transmittance measurements also followed the expected distribution of decreasing changes as the angle between the sample location and nozzle axis increased. The trend exhibited by the optical damage distribution indicated greater damage at large angles (55°) off the nozzle axis than would be predicted by the plume gas flow distribution. At a wavelength of 0.2μm, transmittance changes of at least 10 per cent were measured for an angle of 85 degrees. At an angle of 5 degrees transmittance

changes as large as fifty per cent were measured.

The optical damage data also indicated that somewhat greater damage were measured for the experiment with the shorter ON-time firing pulse (14 msec as compared to the 50 msec).

REFERENCES

1. Jack, J.R., Spisz, E.W., and Cassidy, J.F., "The Effect of Rocket Plume Contamination on the Optical Properties of Transmitting and Reflecting Materials," Paper 72-56, Jan. 1972, AIAA, New York, N.Y.

2. Sommers, R.D., Raquet, C.A., and Cassidy, J.F., "Optical Properties of Thermal Control Coatings Contaminated by MMH/N_2O_4 5-Pound Thruster in a Vacuum Environment with Solar Simulation," Paper 72-163, Apr. 1972, AIAA, New York, N.Y.

3. Spisz, E.W., Bowman, R.L., and Jack, J.R., "Effects of a Bipropellant Thruster Plume on Spacecraft Materials and Optical Components," TM X-68212, 1973, NASA, Cleveland, Ohio.

4. Bowman, R.L., Spisz, E.W., and Jack, J.R., "Effect of Contamination on the Optical Properties of Transmitting and Reflecting Materials Exposed to a MMH/N_2O_4 Rocket Exhaust," TM X-68204, 1973, NASA Cleveland, Ohio.

5. Sommers, R.D., and Raquet, C.A., "Effect of Thruster-Exhaust Damage to S13G White Thermal Control Coatings," TM X-68213, 1973, NASA, Cleveland, Ohio.

6. Cassidy, J.F., "Space Simulation Experiments on Reaction Control System Thruster Plumes," Paper 72-1071, Nov. 1972, AIAA, New York, N.Y.

7. Bowman, R.L., Spisz, E.W., Sommers, R.D., and Jack, J.R., "Skylab Plume Contamination Effects," Paper presented at the Seventh AIAA-ASTM/IES Space Simulation Conference, Los Angeles, Calif., Nov. 1973.

8. McKeown, D., and Corbin, W.E., Jr., "Space Measurements of the Contamination of Surfaces by OGO-6 Outgassing and their Cleaning by Sputtering and Desorption," Space Simulation, J.C. Richmond, ed., SP-336, Oct. 1970, National Bureau of Standards, Washington, D.C., pp 113-127

9. Chuan, R.L., "Particulate Measurement by Quartz Crystal Microbalance," Space Simulation, J.C. Richmond, ed., SP-336, Oct. 1970, National Bureau of Standards, Washington, D.C., pp. 105-111.

REFERENCES (cont'd)

10. Wallace, D.A., "Use of the Quartz Crystal Microbalance for Outgassing and Optical Contamination Measurements," Journal of Vacuum Science and Technology, Vol. 9, No. 1, Jan./Feb. 1972, pp. 462-466.

11. Anon., "Operating Manual for Deposit Thickness Monitor DTM-4," 1971, Sloan Technology Corp., Santa Barbara Calif.

12. Webber, W.T., Hoffman, R.J., and Nunn, J.R., "Analysis of Potential Plume Contamination Effects Resulting from Two 300-Pound Bipropellant Engines Operating in a Satellite Environment," MDC-G3693, AFRPL-TR-72-66, AD-746306, June 1972, Mc Donnell-Douglas Astronautics Co., Huntington Beach, Calif.

13. Hill, J.A.F., and Draper, J.S., "Analytical Approximation for the Flow from a Nozzle into a Vacuum," Journal of Spacecraft and Rockets, Vol. 3, No. 10, Oct. 1966, pp. 1552-1554.

14. Chirivella, J.E., "Mass Flux Measurements and Correlations in the Back Flow Region of a Nozzle Plume," Paper 73-731, July 1973, AIAA, New York, N.Y.

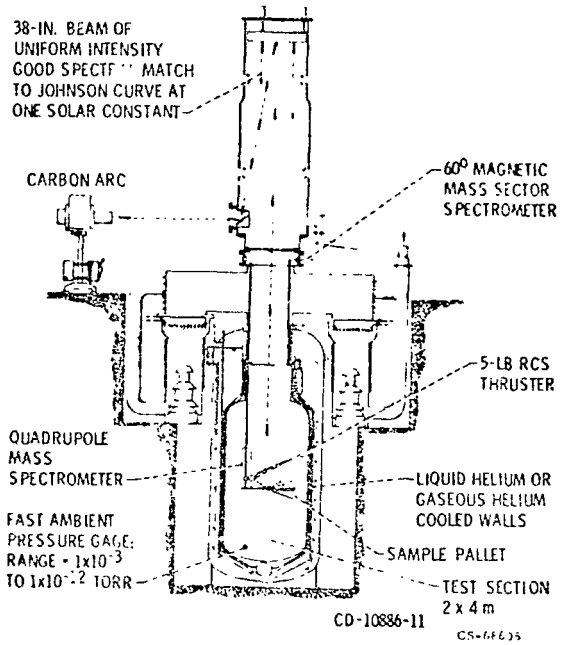

Figure 1. - In-situ rocket plume effects facility.

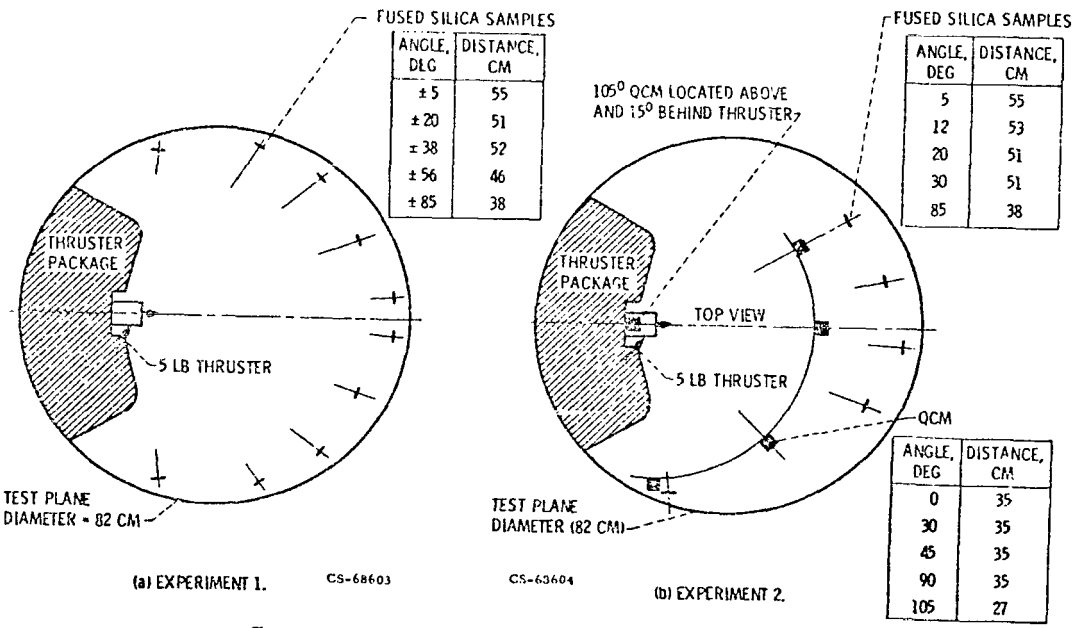

Figure 2. - Test plane. (All samples located on engine centerline elevation.

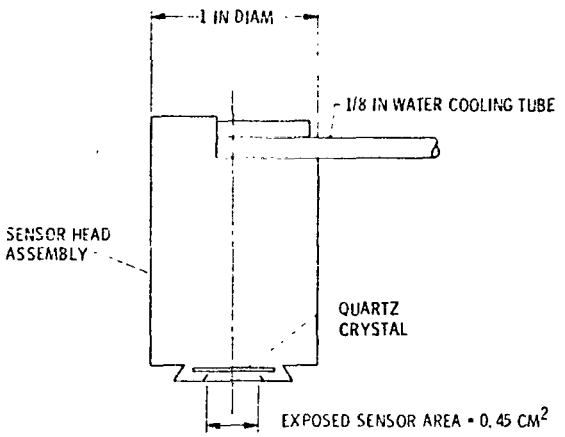

Figure 3. - Quartz crystal microbalance

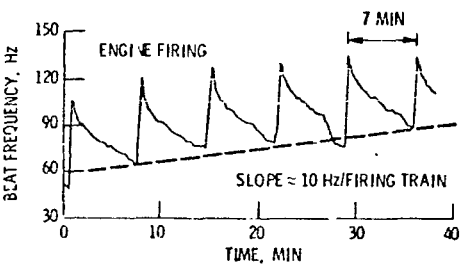

Figure 4. - Typical stepwise response of QCM at 45^0 location for six consecutive firing trains. (Exp 2 data, 14 m sec pulse).

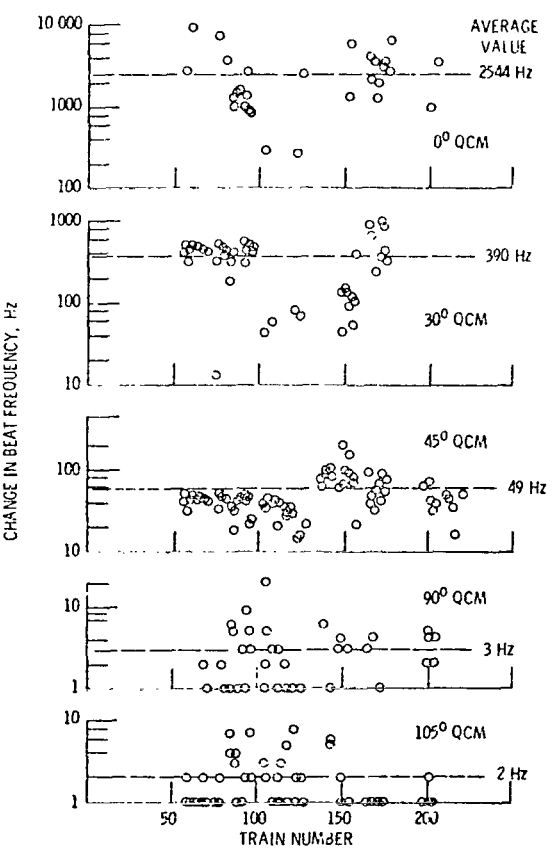

Figure 5. - Change in intial beat frequency. (Exp. 2, 14 m sec pulse data).

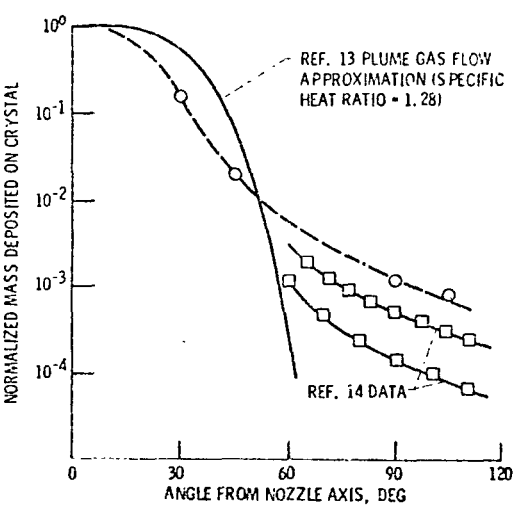

Figure 6. - Normalized plume deposition distribution. (Exp. 2, 14 msec pulse data).

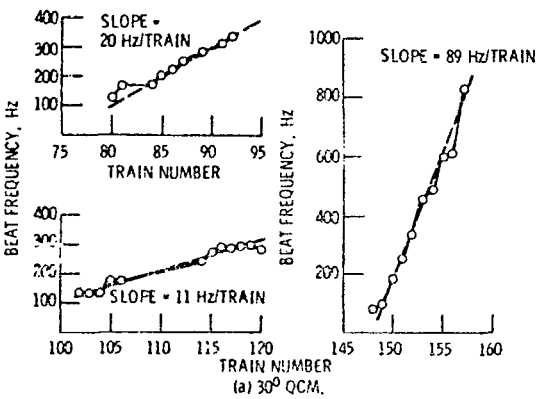

(a) 30° QCM.

Figure 7. - Residual mass deposition measurements. (Exp. 2, 14 m sec pulse).

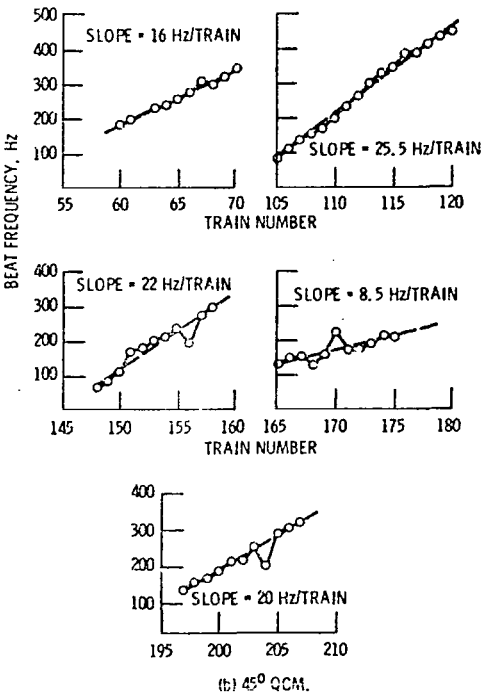

(b) 45° QCM.

Figure 7. - Continued.

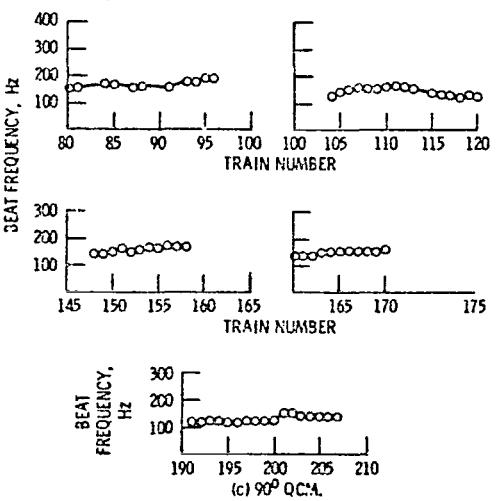

(c) 90° QCM.

Figure 7. - Concluded.

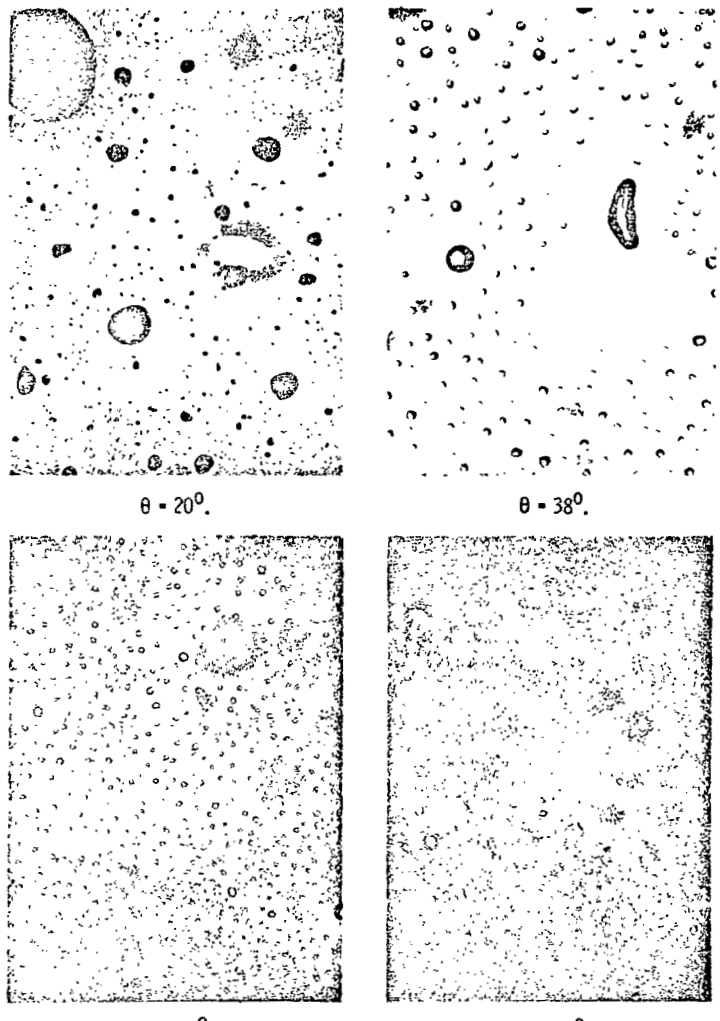

Figure 8. - Photograph of contaminated samples. Experiment number 1. X40.

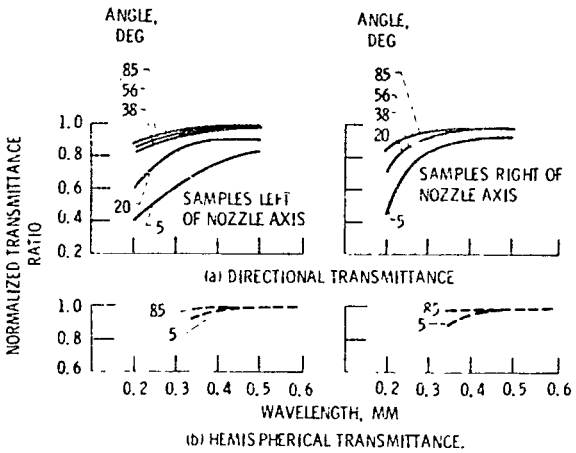

Figure 9. - Transmittance effects. Exp. 1, 50 msec pulse.

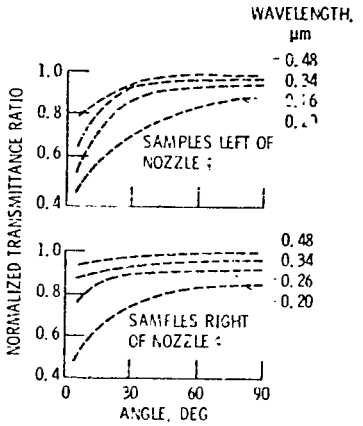

Figure 11. - Optical damage distribution. Directional transmittance data. Exp. 1, 50 msec pulse.

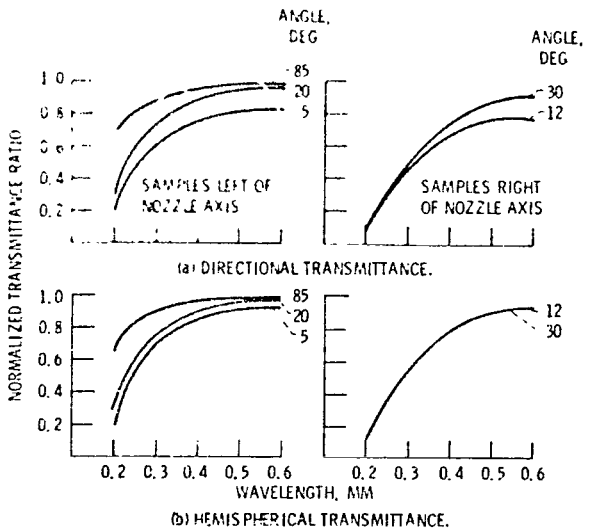

Figure 10. - Transmittance effects (Exp 2, 14 msec pulse).

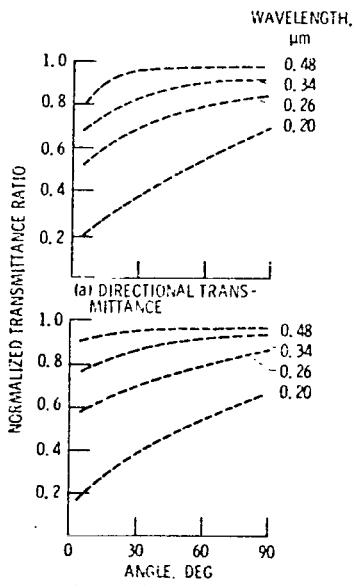

Figure 12. - Optical damage distribution. Exp. 2, 14 msec pulse.

END

DATE

FILMED

JAN 14 1974